A Numerical Analysis of Latent Thermal Energy Storage for Refrigerated Trucks

Michele CALATI[1], Claudio ZILIO[1], Giulia RIGHETTI[1], Giovanni A. LONGO[1], Kamel HOOMAN[2], Simone MANCIN[1,*]

[1]University of Padova, Department of Management and Engineering, Vicenza, 36100, Italy
michele.calati@phd.unipd.it, claudio.zilio@unipd.it, giulia.righetti@unipd.it, tony@gest.unipd.it, simone.mancin@unipd.it

[2]Queensland Geothermal Energy Centre of Excellence School of Mechanical and Mining Engineering University of Queensland, Brisbane, Queensland 4072, Australia
k.hooman@uq.edu.au

* Corresponding Author

ABSTRACT

In this work, an innovative insulated wall concept for refrigerated truck is proposed. A 2D transient numerical model of the truck cell is developed and simulated considering the solar radiation from 6 AM to 4 PM of a typical summer day in Vicenza (Italy). The innovative composite wall consists of a traditional polyurethane (PU) insulation layer wrapping a layer of PCM (reference melting temperature of 2 °C) with different thickness from 0.5 cm to 2 cm. The results confirm that the proposed solution is very promising because even the smallest thickness can assure an adequate temperature inside the cell for almost the entire simulated journey.

1. INTRODUCTION

On global scale, it has been evaluated that about 30% of fresh products are lost because of the optimal distribution temperature is not maintained during the route (Du *et al.*, 2020). Currently, there are about 4 million of vehicles for the refrigerated transport worldwide, which are expected to grow of 2.5% units per year up to 2030 (Glouannec *et al.*, 2014). At the same time, it must be considered that the necessary energy requested for the food transportation only is about 40% of the total amount of energy consumed during transportation (Michel *et al.*, 2017). In the last years, the role of transportation within the cold chain has become more and more important because of the fast increase of global population and the growth of food quantities and varieties. In particular, the demand for fresh food has recently remarkably increased (Du *et al.*, 2020). Fresh products, if compared with frozen ones, are more temperature sensitive (Fioretti *et al.*, 2016). In fact, during the transportation, the foodstuff is subjected to its metabolic activity which affects the ripening rate. Hence, it is essential to maintain the food temperature within a certain range during the entire transport route to ensure the freshness, quality and nutritional value of the delivered products. In this scenario, refrigerated transport systems aim at keeping the temperature at a constant level during their standard operations. Currently, considering the refrigerated road transports, the fleet is for the most part equipped with low efficiency diesel engines for running a mechanical vapor compression cycle for refrigeration (Liu *et al.*, 2012). About 30% of refrigerated road vehicles consist of trailers, 30% of large trucks and 40% of small trucks and vans (Glouannec *et al.*, 2014). Generally, an on-board refrigeration system has a lower performance compared with a stationary one. This is due to the reduced available space on-board on top of various and, in most cases, harsh operating conditions faced during transport. Moreover, the coefficient of performance (COP) usually ranges from 0.5 to 1.5 (Tassou *et al.*, 2009) for such mobile refrigerants. The low engine efficiencies cause a great amount of greenhouse gas emissions, consequently. The ATP ("Accord du Transport Perissable") agreements regulate all the standards for the refrigerated vehicles involved in the transport of perishable foodstuffs. In particular, the ATP classifies the insulated refrigerated vehicles in IN (normal insultation) or IR (reinforced insulation) if their overall heat transfer coefficient ranges between 0.4 and 0.7 W m^{-2} K^{-1} for the former or if it is lower than 0.4 W m^{-2} K^{-1} for the latter. Aiming at reducing energy consumption and assuring the adequate temperature level for the products, researchers have been considering the introduction of Latent Thermal Energy Storage (LTES) systems to replace the traditional designs. The LTES system

takes advantage of the high energy density which can be stored through the phase change process from liquid to solid (or vice versa). An ideal PCM should have a suitable phase change temperature along with high thermal conductivity and latent heat. It should have low volume expansion and large density in order to limit the system size. The PCM should also be compatible with other construction materials that is no toxicity and flammability (Sharma *et al.*, 2009). Focusing on LTES systems for refrigerated transport applications, the pioneering study was conducted by Ahmed *et al.* (2010). They integrated copper tubes filled with paraffin-PCM inside the traditional insulated PU wall of truck trailers. The authors obtained an average reduction of 29.1% of the peak heat flux transmitted to the refrigerated room, demonstrating the great potential of this new technology. Liu *et al.* (2012) developed an innovative on-vehicle LTES unit charged by a stationary refrigeration unit in depot during the night. With respect to a conventional system, the proposed LTES one can account for 86.4% of energy cost savings, with remarkable reduction of greenhouse gas emissions and noise. A similar system was numerically studied by Liu *et al.* (2014). The heat transfer fluid could flow between the cooling unit inside the refrigerated space and the PCTSU (Phase Change Thermal Storage Unit), maintaining the refrigerated space temperature at -18 °C for the entire 10 h truck journey. Copertaro *et al.* (2016) investigated the application of PCM to a 20' ISO container envelope. Compared with the traditional insulated container, the new solution permitted the shift and reduction of the daily peak heat load of 20%, with a heat flux reduction of 4.65%. Tinti *et al.* (2014) analyzed the integration of PU-foam with micro-encapsulated PCM (n-tetradecane, melting temperature 6 °C) through a thermographic analysis. They found that the composite-foam would be suitable for refrigerated transport applications. Glouannec *et al.* (2014) developed a new insulation wall for refrigerated vans using PCM (*Energain*), aerogel and a reflective multi-foil layer. They verified that ATP criteria are not sufficient to estimate the wall heat transfer coefficient, since the regulation doesn't consider other external factors such as solar irradiation. So, the authors added solar irradiation to their analysis and noted that the peak of transferred energy could be increased by up to 43%. The use of aerogel and multi-foil layers, instead, could decrease the effect of solar irradiation by 27%. Michel *et al.* (2017) developed a multi-layer insulation wall made by a layer of PU-PCM foam for refrigerated vehicles. They found that the location of the composite layer influenced the amount of energy crossing the inner face. More recently, Du *et al.* (2020) evaluated the cooling performance of a portable box as a PCM-cold thermal energy storage system. They studied the effects of different PCM modules locations, PCM melting temperatures and insulation materials on the cooling duration length. The PCM equally distributed on the top and side walls led to the longest cooling time.

In this paper, the design of a novel insulated wall for refrigerated vehicles is reported. More specifically, the addition of a PCM layer (with different thicknesses) to the traditional 5 cm insulated PU wall and its ability in maintaining a proper air temperature inside the cell is analyzed. The commercial paraffin wax RT2HC is investigated. In the numerical simulations, run by means of the CFD software Ansys Fluent 18.2, the external solar irradiation was taken into consideration where the hourly solar irradiation profile of a typical Italian summer day was used as input to the simulation. These preliminary results refer to a reference case in which it was hypothesized that no door-openings occurred during the journey and the refrigerated cell was considered empty of freight.

The results are very promising since even the smallest thickness of the PCM layer can ensure the temperature stability inside the truck cell for the most part of the daily journey.

2. NUMERICAL MODEL

2.1 Model description and boundary conditions

As can be observed from Fig. 1, the present work investigated the thermal behaviour of an innovative LTES system involving PCMs. In particular, a novel insulation wall consisting of the traditional PU foam insulation layer and an additional layer filled with a PCM is proposed and studied. The PCM is uniformly distributed on the ceiling and on the side of the refrigerated cell.

In order to simplify the simulations, a 2D section (2.4 m x 2.6 m) of a semi-trailer insulated rigid box was taken as our computational domain. This type of refrigerated vehicle is the most popular in Europe. Its external width and length are fixed: 2.6 m and 13.56 m, respectively (Tassou *et al.*, 2009). As reported by the same authors, the insulation thickness is limited because it comes from the trade-off between the maximum admissible vehicle width (2.6 m) and the Europallet's dimensions (1 m deep x 2 m width). If 2 Europallets are located side by side in the refrigerated cell the insulation layer can rarely be more than 5 cm thick.

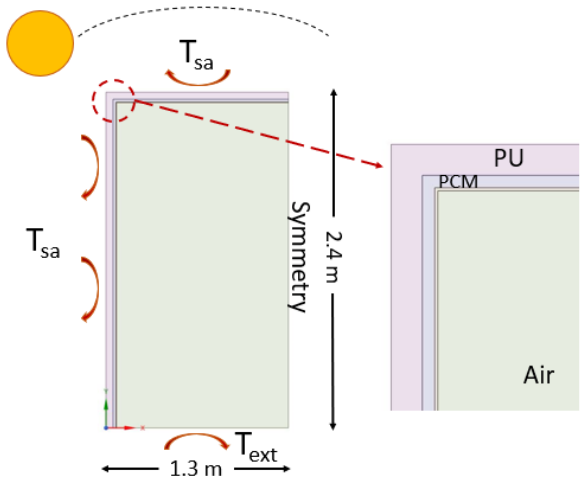

Figure 1. Model description and boundary conditions

Hence, for the numerical simulations, a 5 cm thick PU-layer was chosen. To evaluate the ability of PCM in counteracting the heat loads transmission into the refrigerated cell, different PCM layer thicknesses were selected, ranging between 0.5 cm and 2 cm. An aluminum encapsulation layer of 0.5 cm was located between the PCM and the air, as demonstrated in Fig. 1. The thermo-physical properties of the materials and PCMs are reported in Table 1 and 2, respectively.

Table 1: Material main properties

Material	**k** [W m^{-1} K^{-1}]	**ρ** [kg m^{-3}]	**C_p** [J kg^{-1} K^{-1}]
Poly-Urethane foam	0.03	35	1380
Aluminum	202.4	2719	871

Table 2: Phase Change Materials main properties

PCM	**k** [W m^{-1} K^{-1}]	**ρ_{sol}/ ρ_{liq}** [kg m^{-3}]	**C_p** [J kg^{-1} K^{-1}]	**L** [kJ kg^{-1}]	**$T_{solidus}$/$T_{liquidus}$** [°C]
RT2HC	0.2	880/770	2000	200	1/3

To take into account the effect of the solar irradiance on the top and on the side of the truck, the sol-air model was applied which is popular in simulations involving heat transfer problems for buildings (Villi *et al.*, 2009). A fictitious free stream temperature T_{sa} is calculated, as Eq. (1) below, to consider the convective and radiative contributions to the energy transfer:

$$T_{sa} = T_{ext} + \frac{G_{\beta t} * a}{\alpha} \quad (1)$$

The absorptance a was fixed at 0.5, while a global heat transfer coefficient α of 10 W m^{-2} K^{-1} was selected. For each truck surface, the solar irradiance $G_{\beta t}$ was obtained following the procedure described in section 2.2.1.
To simplify the numerical analysis, only half of the entire section was simulated. Therefore, as can be observed from Fig.1, a "symmetry" condition was applied to the symmetry axis of the 2D truck section. The truck was oriented considering the opening doors facing South. It implies that the cell sides were oriented to the West or to the East. However, due to the symmetry condition, only the T_{sa} calculated for the West-oriented face was used for the cell side. It permitted to study the worst-case scenario because the calculated temperatures for the western face were always higher than those of the eastern one. At the bottom of the cell a global heat transfer coefficient of 0.7 W m^{-2} K^{-1} was applied which took into account the conductive heat transferred through 5 cm PU insulation layer and the convective coefficient of 7 W m^{-2} K^{-1} (Glouannec *et al.*, 2014) considering a free stream temperature equal to the ambient temperature T_{ext}. The initial air temperature inside the refrigerated cell was set to 2 °C for all simulated conditions. The PCM was initially fixed at a temperature 0.5 °C lower than the $T_{solidus}$ of each PCM, in order to assure that the PCM was totally solid at the beginning of the simulation. The volume averaged air and PCM temperature were monitored and analysed to describe the LTES' behaviour. Besides, the temperature distribution inside the truck cell was investigated.

2.2 Governing Equations

2.2.1 Incident Solar Irradiance Estimation

For the entire simulated truck journey (from 6 AM to 4 PM) the hourly solar heat on each truck surfaces was estimated. To simulate the worst case scenario, data for a typical Italian summer day were considered. A representative average day of July (n = 196) was chosen because from historical data-series it was observed that July is the warmest month in Italy. The climate data available here www.try.cti2000.it (Italian Thermo-Technical Committee site) are used for our simulation. For each day of the year, the temperature, the hourly beam and diffusive radiations on a horizontal surface can be downloaded.

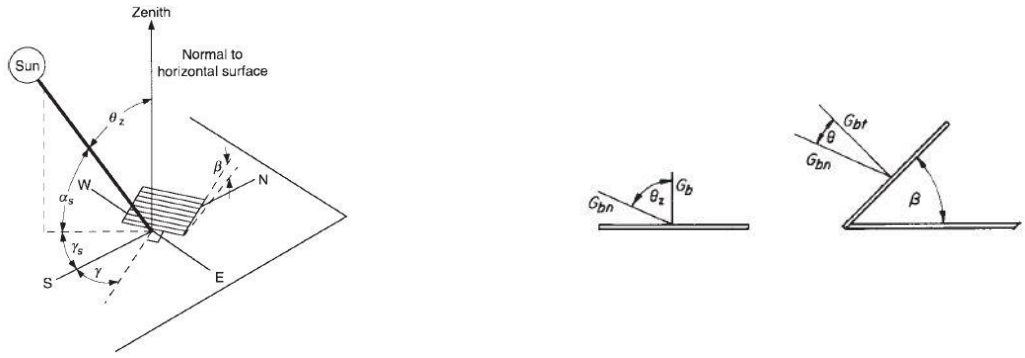

a) b)

Figure 2. The most significant solar variables for a tilted surface (a), global radiation on a tilted surface (b). Images taken from Duffie and Beckman (2013)

The following equations were adapted from Duffie and Beckman (2013), in order to estimate the hourly global radiation on a tilted surface (Fig. 2b)
The first step was the calculation of the solar time as reported in Eqns. (2-4), for obtaining the solar angle (5):

$$SolarTime - StandardTime = 4(M_{st} - M_{loc}) + E \quad (2)$$

$$E = 229.2(0.000075 + 0.001868\cos(B) - 0.032077\sin(B) - 0.014615\cos(2B) - 0.04089\sin(2B)) \quad (3)$$

$$B = (n-1)\frac{360}{365} \quad (4)$$

$$\omega = 15(SolarTime - 12) \quad (5)$$

The second step involved the estimation of the Zenith (7) and solar Azimuth (8) angles after having calculated the solar rays' declination (6):

$$\delta = 23.45sen(360\frac{284+n}{365}) \quad (6)$$

$$\theta_z = cos^{-1}(cos\phi cos\delta cos\omega + sin\phi sin\delta) \quad (7)$$

$$\gamma_s = sign(\omega)\left|\frac{cos\theta_z sin\phi - sin\delta}{sin\theta_z cos\phi}\right| \quad (8)$$

Knowing the Zenith and solar Azimuth angles, surface tilt and Azimuth angles, the angle of incidence of the beam radiation could be predicted as follows:

$$\theta = cos^{-1}[cos\theta_z cos\beta + sin\theta_z sin\beta\cos(\gamma_s - \gamma)] \quad (9)$$

Finally, for each truck surfaces the global radiation could be calculated:

$$G_{\beta t} = G_b\frac{cos\theta}{cos\theta_z} + G_d \quad (10)$$

2.2.2 Solving equations

The commercial CFD software "Ansys Fluent 18.2" was used to run the numerical simulations. The "Solidification and Melting Model" was adopted to investigate the transient behaviour of the LTES system. The model takes advantage of an enthalpy-porosity approximation of the zone involved in the phase change process, denoted as mushy zone. In fact, the liquid-solid mushy zone is considered as a porous one and the porosity is set as the liquid fraction. This latter is a quantity indicating the fraction of the cell volume in liquid state, calculated for the all cells in the domain. In the mushy region, the liquid fraction ranges between 0 (PCM solid) and 1 (PCM liquid).
Hence, the energy equation Eq. (15) is written in terms of enthalpy Eq. (11), considered as the sum of sensible enthalpy Eq. (12) and latent heat of fusion Eq. (13), as reported in the following equations:

$$H = h + \Delta H \tag{11}$$

$$h = h_{ref} + \int_{T_{ref}}^{T} c_p dT \tag{12}$$

$$\Delta H = \varphi L \tag{13}$$

$$\varphi = \begin{cases} 0, if\ T < T_{solidus} \\ \dfrac{T - T_{solidus}}{T_{liquidus} - T_{solidus}},\ if\ T_{solidus} < T < T_{liquidus} \\ 1, if\ T > T_{liquidus} \end{cases} \tag{14}$$

$$\frac{\partial}{\partial t}(\rho H) + \nabla \cdot (\rho \boldsymbol{v} H) = \nabla \cdot (k \nabla T) + S \tag{15}$$

To develop the momentum conservation equation for the mushy region, a momentum sink is inserted in the Navier-Stokes equation as:

$$\frac{\partial}{\partial t}(\rho \boldsymbol{v}) + \nabla(\rho \boldsymbol{v}\boldsymbol{v}) = -\nabla p + \mu \nabla^2 \boldsymbol{v} + \rho g \epsilon (T - T_{ref}) + \frac{(1-\varphi)^2}{\varepsilon + \varphi^3} A_{mush} \boldsymbol{v} \tag{16}$$

In the right side of Eq. (16), the last two terms stand for the buoyancy force with Boussinesq approximation and the momentum sink, respectively.
Additionally, to analyse the thermal fluid dynamics, the following equations, conservation of mass, momentum and energy are solved:

$$\frac{\partial}{\partial t} \nabla \cdot (\rho \boldsymbol{v}) = 0 \tag{17}$$

$$\frac{\partial}{\partial t}(\rho \boldsymbol{v}) + \nabla(\rho \boldsymbol{v}\boldsymbol{v}) = \nabla p + \nabla(\boldsymbol{\tau}) + \rho \boldsymbol{g}(T - T_{ref}) + \boldsymbol{F} \tag{18}$$

$$\frac{\partial}{\partial t}(\rho E) + \nabla \cdot \left[\boldsymbol{v}(\rho E + p)\right] = \nabla \cdot \left[k_{eff} \nabla T - \sum_{\boldsymbol{i}} h_i \boldsymbol{j_i} + (\boldsymbol{\tau_{eff}} \cdot \boldsymbol{v})\right] + S_h \tag{19}$$

The second order upwind scheme was adopted to linearize the convective terms with first order derivatives, while the diffusive terms with second order derivatives were linearized by a second order differencing scheme. The SIMPLE scheme was used to solve the pressure-velocity coupling while the PRESTO! one was chosen for pressure correction, as proposed by Zhao *et al.* (2020). All of the other equations were linearized using the algebraic multigrid (AMG) iterative strategy.

2.3 Sensitivity Analyses and Model Validation

2.3.1 Time Step and Mesh Sensitivity Analyses

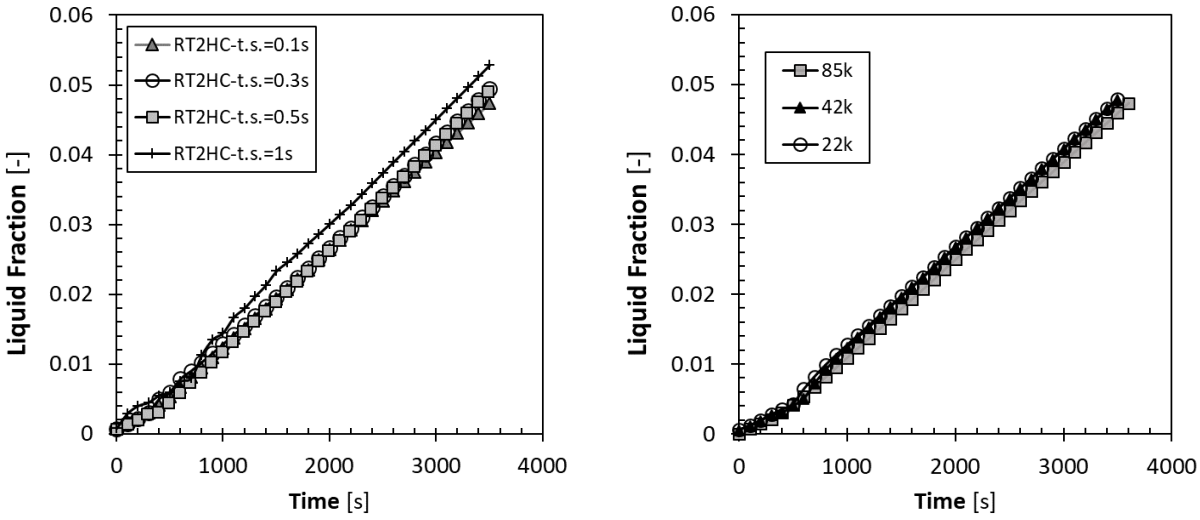

Figure 3. a) Time Step Sensitivity Analysis, b) Mesh Sensitivity Analysis

To evaluate the influence of the time step and calculation grid sizes on the numerical solution, two different sensitivity analyses were conducted. The liquid fraction at the end of the first simulated hour (3600 s) was chosen as parameter aiming at comparing different results. Among the three investigated configurations, RT2HC and 0.5 cm PCM thick layer were used for the sensitivity analyses, since it was considered the most stringent case. As reported in Fig. 3a, when the time step size changes from 0.1 to 0.5 s a noticeable difference between the curves cannot be appreciated. While the curves for 0.1, 0.3, 0.5 s time step size mostly overlap, the curve for time step set to 1 s (RT2HC-t.s.=1s) shows a different behaviour. Therefore, a time step size of 0.5 s was selected for all the numerical analyses. In Fig 3b, the grid independence analysis is shown. To find the optimal trade-off between computational efforts and solution robustness, three different meshes were studied (22k, 42k, 85k elements). From 85k to 22k number of elements, no differences can be noted, confirming the grid independence of the solution, even if the computational time dropped from 2.5 h to 1.2 h, respectively. However, since meshes of 22k and 42k had similar computational time, the latter (Fig. 4) was used for all the other analyses.

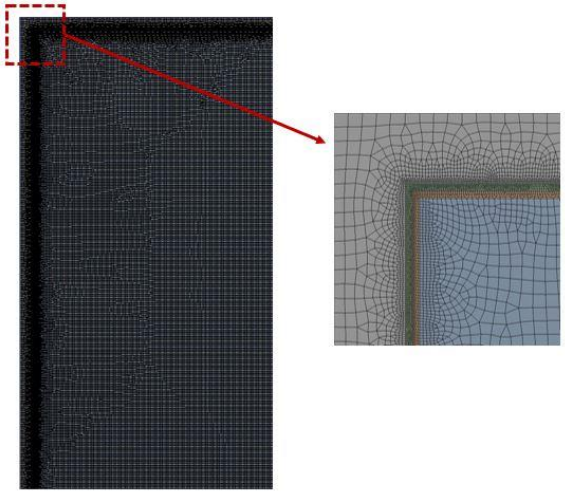

Figure 4. Mesh of 42k elements. Details.

2.3.2 Model Validation

Glouannec *et al.* (2014) studied an insulation wall made of 0.1 cm of metal sheet (denoted as "Body"), an air gap of 10 cm, 0.1 cm of fiberglass, 5.8 cm of polyurethane and 0.2 cm of polyester and fiberglass. The insulation wall was 86 cm tall. They applied a constant free stream external temperature of 10 °C for the first 4 simulation hours and 30 °C for the last four. The insulation wall was installed in a climatic adiabatic room maintained at 0 °C. They validated their numerical model against experimental results. Therefore, the present authors reproduced similar conditions and obtained results comparable to those reported by Glouannec *et al.* (2014), as shown in Fig. 5.

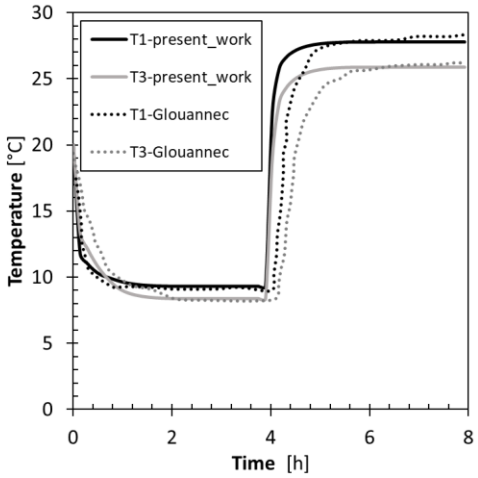

Figure 5. Comparison between present results and what obtained by Glouannec *et al.* (2014)

T1 and T3 were the temperatures at mid-height of the inner side of the bodywork and of the outer side of the fiberglass layer, respectively. As can be seen in Fig. 5, the present numerical model was able to fairly reproduce the experimental data in Glouannec *et al.* (2014). Since the presence of the external bodywork and of the internal polyester + fiberglass layers were not considered here a slightly different temperature at the fourth hour can be noted. In fact, during the change of the external conditions (from 10 °C to 30 °C external temperature) a faster transition occurred, due to the reduced thermal capacity.

3. RESULTS AND DISCUSSION

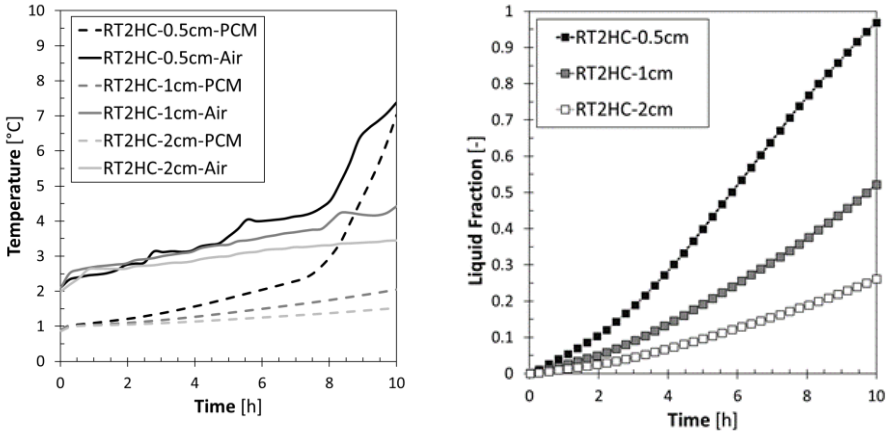

a) b)

Figure 6. a) Volume-averaged PCM and air Temperature, b) Liquid Fraction, for three different PCM layer thicknesses

In Fig. 6a, the volume-averaged PCM temperature and air temperature for the three paraffin-based PCMs investigated with three different PCM layer thicknesses (0.5, 1, 2 cm) are plotted. The ability of the LTES system in maintaining the air temperature inside the cell as closely as possible to the ideal melting PCM temperature without the use of refrigerated system was demonstrated.

As shown in Fig. 6a, the 0.5 cm RT2HC layer permitted to maintain the air temperature inside the refrigerated cell below 3 °C for the first 4 h. This threshold is the *liquidus* temperature of RT2HC: it means that when the temperature exceeds 3 °C the PCM is fully liquid locally. For the next 4 h, the air temperature ranges between 3 and 4 °C, while, at the ninth simulated hour a sharp temperature increase is noted. In fact, from the end of the eighth hour till the end of the simulated truck journey, an evident change of slope for the air temperature curve can be appreciated. Between the seventh and the eighth hour, a sudden PCM mean temperature rise can be observed, as shown by the black dotted line plotted in Fig. 6a. Comparing the PCM temperature curve with the liquid fraction one (Fig. 6b, black line), it can be noted that for the most part of the melting process (about 8 h, *i.e.* 85% liquid) the PCM temperature was maintained between the *solidus* and *liquidus* temperatures. Therefore, the ability to limit the heat load to be transmitted inside the refrigerated cell is weakened as the PCM almost completely melted. The sharp rise in the PCM temperature reflected in the increase of air temperature, up to 7 °C, is because of the sensible heat transfer to liquid PCM. This can potentially be detrimental for fresh foods which must be transported and delivered at temperatures around 2-3 °C. Hence, a design with thicker layer was investigated. Focusing on Fig. 6a, a similar trend in the air temperature curve for the 1 cm and 0.5 cm can be noted during the first 4 h of the simulation. Nevertheless, from the 4th h till the 10th hour the curve slope is steeper for the 1 cm PCM layer scenario with no air temperature rise. In fact, studying the mean PCM temperature curve trend (dark grey dotted line, Fig. 6a), it is evident that RT2HC temperature was in the melting range for the entire simulated truck journey. In fig. 6b, it is shown that only some 53% of PCM melted at the end of the simulation. However, the air temperature stabilized at about 1°C above the *liquidus* temperature, *i.e.* at 4.2 °C, during the last 2 hours. If the temperature requirements are not so strict for the carried foodstuff, the 1 cm configuration can be considered as the best one. On the contrary, for more temperature sensitive products, a thicker layer can be used. Therefore, the PCM layer was increased to 2 cm. In this scenario, the air temperature curve assumed a different trend, as plotted in Fig. 6a (light grey line). It flattened asymptotically along the *liquidus* temperature threshold. After ten simulated hours, only a quarter of RT2HC melted, as shown in Fig. 6b, and an air temperature of 3.4 °C was reached. The air temperature curve trend and the amount of liquid fraction suggest the LTES with 2 cm layer behaviour to be suitable for a prolonged truck route. However, this suggestion will be investigated in future works.

For the LTES system with 0.5 cm RT2HC layer, the temperature distribution inside the refrigerated cell can be appreciated in Fig. 7. In particular, in Fig. 7a the temperature distribution during the first two hours of the simulated route is visualized.

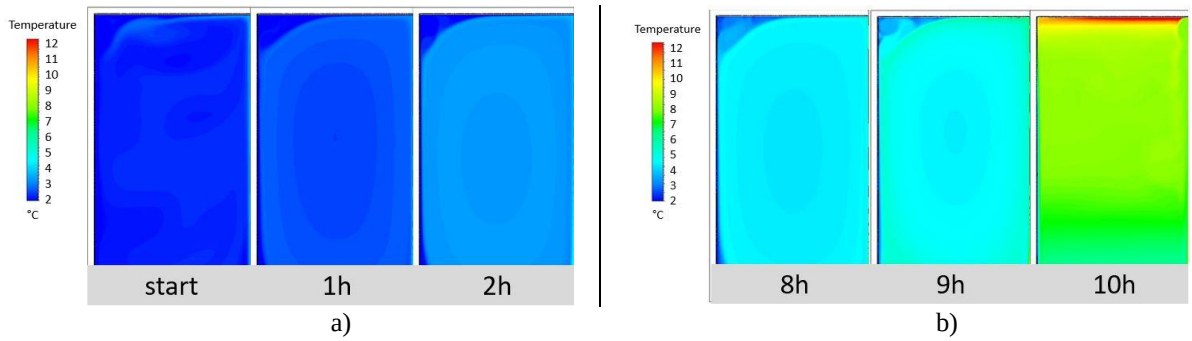

a) b)

Figure 7. Air temperature contours inside the refrigerated cell a) at the early stages, b) at the final stages for the LTES system with 0.5 cm RT2HC layer

As can be observed, different isothermal circular layers were formed. In fact, the air, being heated up from the bottom of the cell, moved upwards. When the cell ceiling was reached, the air was cooled down by the PCM which was at a lower temperature (see Fig. 6a) and moved downwards. These convective movements continued until an appreciable temperature gradient between the air and PCM existed. In Fig. 7b the air temperature behaviour during the last three simulated hours is shown. As shown in Fig. 6a, after the 9th hour, the PCM temperature curve approached the air one. This caused the temperature gradient between air and PCM to be almost null and the air movement to become less intensive, consequently. In particular, as shown in Fig. 7b, during the last hour, a horizontal temperature stratification occurred. The air in the upper part was warmer (about 12 °C) if compared to air close to the side of the cell.

The PCM at the uppermost part of the cell ("Top") is completely melted, justifying a greater PCM temperature (and of the closest air, consequently). The RT2HC along the side of the cell ("Side") was not melted at all during the tenth hour. In fact, a liquid fraction ranging between 85% and 90% can be found, as shown in Fig. 8a. The PCM contained in the top enclosure of the cell reached the end of melting process during the ninth hour, whilst the PCM contained in the side one was at 92% of liquid fraction at the end of the 10th hour, as can be observed by the curves reported in Fig. 8b.

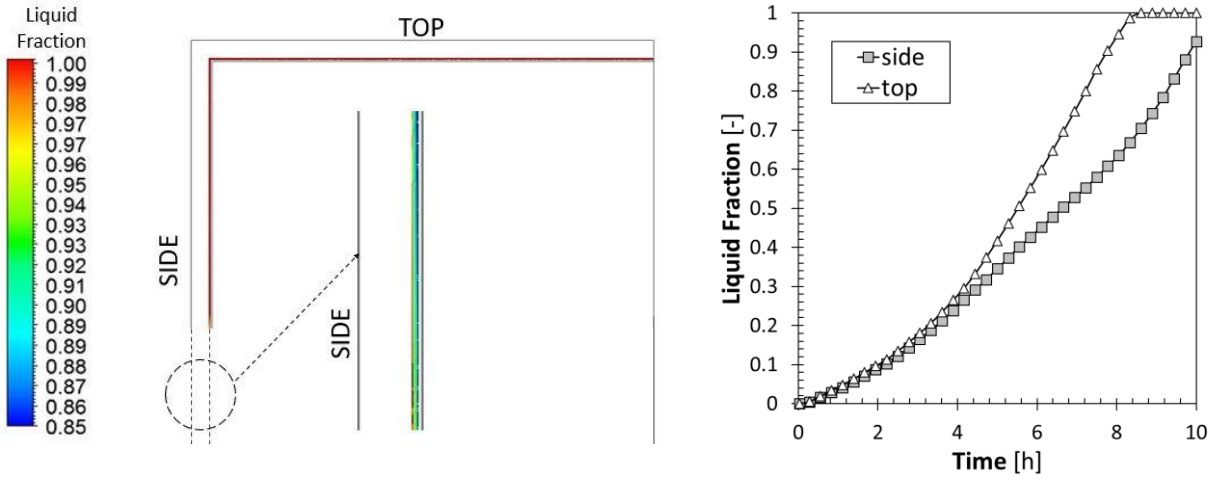

a) b)

Figure 8. a) Liquid fraction contours at the 10th hour, b) Liquid fraction trend, for the side and top of the refrigerated cell

4. CONCLUSIONS

In this work, a novel insulated wall for refrigerated transport consisting of a PU layer and a PCM one was investigated. A 2D section of a refrigerated truck was modelled. The hourly solar irradiance profile was obtained for a typical summer Italian day aiming at estimating and applying the external heat loads on a reference 10 h truck daily route. By means of CFD numerical simulations, the effect of incorporating a RT2HC PCM layer in a traditional 5 cm polyurethane insulation layer was studied. Specifically, the additional PCM layer thickness ranged between 0.5 cm and 2 cm. Its ability in maintaining the air temperature in the refrigerated space for fresh food transportation at a suitable level without the use of refrigeration systems were analysed. The results showed that the temperature glide during the phase change affected the thermal behaviour of the LTESs. In particular, the 0.5 cm PCM layer assured an air temperature lower than the *solidus* temperature only for the first four simulated hours. Then, the air temperature stabilized at about 1 °C over the *solidus* temperature and then, when the PCM was almost fully melted, a sudden temperature increase occurred, which would be potentially detrimental for high-sensible foodstuffs. The 1 cm layer, instead, let the air temperature to be no more than 2 °C higher than the PCM reference melting temperature for the entire 10h simulated truck journey. Among all the other investigated layers, the thickest one assured the most uniform air temperature during the route. Since, with the 2 cm layer, only some 25% of PCM melted, an extension of the truck journey will be simulated in future numerical investigation. Besides, after the preliminary simulations here presented, the presence of cold freight, heat respiration and heat infiltrations will be considered in the next analyses, in order to find the optimal LTES design.

NOMENCLATURE

a	absorptance, [-]	PU	Polyurethane	φ	liquid fraction, [-]
ATP	Accord du Transport Perissable	RT	Rubitherm ®	ϕ	latitude, [°]
B	variable, [-]	S	source term	ω	solar angle, [°]
C_p	Heat Capacity, [J kg^{-1} K^{-1}]	v	velocity, [m s^{-1}]		**Subscripts**
E	variable, [min]		**Greek Symbols**	b	beam
F	external force, [N]	α	heat transfer coefficient, [W m^{-2} K^{-1}]	d	diffuse

G	solar irradiance, [W m^{-2}]	α	altitude, [°]	ext	external
h	enthalpy, [J]	β	tilt angle, [°]	liq	liquid
k	thermal conductivity, [W $m^{-1}K^{-1}$]	γ	azimuth angle, [°]	loc	location
L	Latent Heat, [J kg^{-1}]	δ	solar declination, [°]	s	solar
LTES	Latent Thermal Energy Storage	ϵ	thermal expansion coefficient, [K^{-1}]	sa	sol-air
M	meridiane	θ	angle of incidence, [°]	sol	solid
n	day of the year, [-]	μ	dynamic viscosity, [Pa·s]	st	standard
p	pressure, [Pa]	ρ	density, [Kg m^{-3}]	t	total
PCM	Phase Change Material	τ	shear stress tensor	z	Zenith

REFERENCES

Ahmed, M., Meade, O., Medina, M. A. (2010). Reducing heat transfer across the insulated walls of refrigerated truck trailers by the application of phase change materials. *Energy Conversion and Management*, 51, 383-392.

Copertaro, B., Principi, P., Fioretti, R. (2016). Thermal performance analysis of PCM in refrigerated container envelopes in the Italian context - Numerical modelling and validation. *Applied Thermal Engineering*, 102, 873-881.

Duffie, J. A., Beckman, W. A. (2013). Solar Engineering of Thermal Processes. *John Wiley & Sons*, New Jersey.

Du, J., Nie, B., Zhang, Y., Du, Z., Wang, L., Ding, Y. (2020). Cooling performance of a thermal energy storage-based portable box for cold chain applications. *Journal of Energy Storage*, 28, 101238.

Fioretti, R., Principi, P., Copertaro, B. (2016). A refrigerated container envelope with a PCM layer: experimental and theoretical investigation in a representative town in Central Italy. *Energy Conversion and Management*, 122, 131-141.

Glouannec, P., Michel, B., Delamarre, G., Grohens, Y. (2014). Experimental and numerical study of heat transfer across insulation wall of a refrigerated integral panel van. *Applied Thermal Engineering*, 73, 196-204.

Liu, M., Saman, W., Bruno, F. (2012). Development of a novel refrigeration system for refrigerated trucks incorporating phase change material. *Applied Energy*, 92, 336-342

Liu, M., Saman, W., Bruno, F. (2014). Computer simulation with TRNSYS for a mobile refrigeration system incorporating a phase change material storage unit. *Applied Energy*, 132, 226-235.

Michel, B., Glouannec, P., Fuentes, A., Chauvelon, P. (2017). Experimental and numerical study of insulation walls containing a composite layer of PU-PCM and dedicated to refrigerated transport. *Applied Thermal Engineering*, 116, 382-391.

Sharma, A., Tyagi, V. V., Chen, C. R., Buddhi, D. (2009). Review on thermal energy storage with phase change materials and applications, *Renewable and Sustainable Energy Reviews*, 13, 318-345.

Tassou, S. A., De-Lille, G., Ge, Y. T. (2009). Food transport refrigeration - Approaches to reduce energy consumption and environmental impacts of road transport. *Applied Thermal Engineering*, 29, 1467-1477.

Tinti, A., Tarzia, A., Passaro, A., Angiuli, R. (2014). Thermographic analysis of polyurethane foams integrated with phase change materials designed for dynamic thermal insulation in refrigerated transport. *Applied Thermal Engineering*, 70, 201-210.

Villi, G., Pasut, W., De Carli, M. (2009). CFD modelling and thermal performance analysis of a wooden ventilated roof structure. *Building Simulation*, 2, 215-228.

Zhao, C., Opolot, M., Liu, M., Bruno, F., Mancin, S., Hooman, K. (2020). Numerical study of melting performance enhancement for PCM in an annular enclosure with internal-external fins and metal foams, 150, 119348.

ACKNOWLEDGMENT

The authors wish to acknowledge the support and the computational resources made available by the High Performance Computing Lab at the Department of Management and Engineering (DTG), co-funded by the University of Padova in the framework of the program “Scientific research instrumentation 2015”.